Resistivity scaling transition in ultrathin metal film at critical thickness and its implication for the transparent conductor applications

Yong-Bum Park, Changyeong Jeong, and L. Jay Guo*

Department of Electrical Engineering and Computer Science, University of Michigan, Ann Arbor, MI 48109, USA

** Corresponding author. Telephone: 1-734-647-7718; Fax: 1-734-763-9324; Email: guo@umich.edu*

Keywords: Ultrathin metal film, resistivity scaling, size effect theory, general effective media

Abstract

Understanding of ultrathin metal film's electrical and optical properties at sub-10 nm thickness may provide important engineering insight on its application as a transparent conductor. Here, we observe a rapid change in ultrathin metal film's electrical and optical scaling properties as the thickness shrinks to below certain critical thickness d_c. Below this thickness, the metal film's electrical property is shown to be strongly influenced by inhomogeneity of the film which can be modeled via general effective media theory with incorporating size-effect contribution. As a result, below d_c, carrier's scattering time rapidly decreases with reduced mean free path leading to rapid rise in resistivity. Also, the film's optical loss increases while the optical transmission plateaus below d_c. As one promising application of thin metal film is transparent conductor where the film's electrical and optical properties are equally important, we show that its maximum theoretical figure-of-merit is determined at this d_c serving as an important engineering metric.

1. Introduction

Understanding electrical and optical properties of thin metal films serves as foundation for its application in electronic and photonic devices.[1] Recently, metal film with thickness in the ultrathin (< 10 nm) scale has caught great interest because metals such as silver (Ag) or gold is known to have excellent optoelectronic or plasmonic property due to their low resistivity and optical loss.[2, 3] To obtain continuous and ultrathin films of these metals, efforts were made to lower the percolation threshold thickness of these materials by overcoming their intrinsic de-wetting problem.[4, 5] These efforts enabled numerous applications such as transparent conductor, [2, 6, 7] low-loss plasmonic waveguide,[8] EMI shielding,[9] or other nanophotonic applications.[10] [11] In particular, ultrathin metal film[3, 12] has gained great interest over the past years exhibiting advantages including excellent electrical/optical properties with mechanical flexibility and simple fabrication procedure compared to counterparts like metal-oxide films,[13] carbon-based materials,[14] or metal nanowires.[15] Additionally, our recent result shows that ultrathin metal film as a transparent conductor can completely eliminate waveguide mode in organic light emitting device to achieve better device efficiency, outstanding benefit over metal-oxide films.[16] As the apparent electrical resistivity becomes strongly dependent on the film's thickness in this regime, understanding the resistivity change at ultrathin regime may provide insight and guidance in engineering applications. Electrical properties of metal films become a sophisticated problem especially when the thickness is close to extremely thin (~ 5 nm) regime where not only the size effect affecting the resistivity but also the morphological changes of the films starts to strongly influence its electrical property.[17, 18] Despite its significance, research on ultrathin metal films so far mostly involve experimental observation of resistivity scaling[6, 19] with little effort on rigorously investigating how understanding its electrical and optical properties can better serve to guide or solve engineering problems.

Several studies were conducted in the past to understand the morphological evolution of metal film growth and how it impacts the electrical and optical properties of the film at ultrathin regime.[17, 18, 20-22] For example, Zhang et al.[17] discussed the resistivity change of ultrathin Ag film near critical thickness where the transition of growth mode happens, though the basis of defining critical thickness is not clear. Maaroof et al.[18] introduced the term critical thickness near percolation threshold for Pt and Ni thin films by modeling the electrical resistance associated with morphological change of the film. Hovel[22] observed the

optical property change of ultrathin gold film near percolation threshold where metal-to-insulator transition occurs. These studies use the term critical thickness or percolation threshold to better identify the morphological transition of film growth, but they did not provide further insight or practical implication in addressing engineering applications. As a step closer to bridging the gap, Ghosh et al. experimentally demonstrated how the term percolation threshold thickness of metal film can be associated with transparent conductor's optimum figure-of-merit.[20, 21] However, the work is based on experimental observation only and lacking in theory. Although these works help us to understand the film's property at ultrathin thickness regime, it is difficult to find direct correlation on how resistivity modeling or terminologies can help us better design electronic or photonic devices.

We provide a detailed study on the implication of critical thickness d_c at which the sharp transition of electrical resistivity occurs in ultrathin metal films. This transition of resistivity near d_c is explained by using general effective media theory, treating the film as inhomogeneous medium composed of metal film with air voids, which provides excellent fit to the measured resistivity scaling behavior. Based on this analysis, the scientific and engineering implication of d_c is discussed. First, below d_c, drastic increase in electrical resistivity is attributed to the rapid decrease in scattering time, a regime where size effect scattering models no longer dominates. This is explained via film's morphology change that impacts the electron mean free path. Second, optical absorption of the film increases while optical transmission reaches a plateau. Finally, when using such extremely thin metal film as a transparent conductor, its figure-of-merit reaches a maximum value at d_c. This interesting correlation becomes a useful design guideline in designing ultrathin Ag film transparent conductor to improve the efficiency of light emitting device[23] as our recent work shows that waveguiding in OLED can be eliminated.[16]

2. Results and Discussions

2.1. Observation of critical thickness

Ultrathin copper-seeded thin silver film, denoted as Ag (Cu), was prepared according to our previous work.[16] The measured resistivity of Ag (Cu) thin metal films shows exponential increase with decreasing average film thickness d. **Figure 1(a)** shows the log-log plot of measured Ag (Cu) film's resistivity (open symbol) as a function of d. Clearly the resistivity

curve shows two distinct linear regimes in a log-log scale (two dashed-lines are drawn as a guide only), in which the rapid resistivity scaling at lower thickness can be easily overlooked if plotted under linear scale. This double-sloped behavior is quite universal, as it was also observed in Ag films with germanium as seed-layer or even without any seed layer (Figure S1); and can be seen in other metal films like Au,[5] Cu,[24] or NiCr;[25] though none of these works closely examined this phenomenon and its implications. It is worth paying attention to the film's thickness at which two slopes in Figure 1(a) intersect which is marked in vertical red dashed line and will be referred as critical thickness d_c, which is empirically obtained as 5 nm for Ag (Cu) film.

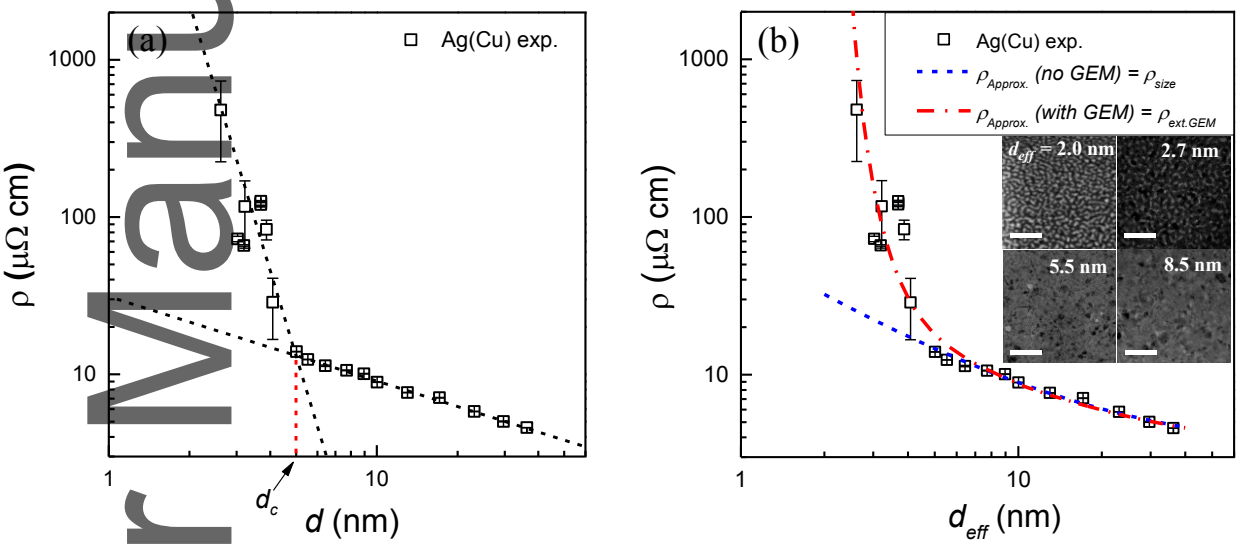

Figure 1. (a) Resistivity ρ of Ag (Cu) film as a function of film thickness d plotted in log-log scale. The open symbols are the measured data while dotted lines extrapolating double-slope behavior of resistivity scaling are not based on any physical model. The critical thickness d_c is indicated as vertical red dotted line which is 5 nm for Ag (Cu) film. (b) ρ versus d approximated by using size effect model only (ρ_{size}) is plotted in blue dashed line and that by extended GEM model ($\rho_{ext.GEM}$) is plotted in red dashed-dot line. Measured experimental resistivity values are plotted in open symbols for reference. Inset images are the top-down TEM images of Ag (Cu) films with thickness d ranging from 2.0 nm to 8.5 nm where corresponding thickness for each image is indicated. Regions appear as light or dark color each correspond to region with air (void) or metal, respectively. All images have scale bar of 50 nm. The images are process to show better contrast between the projected area of metal and air.

2.2. Electrical resistivity approximation

Better understanding of rapid increase in resistivity below d_c is important in designing metal film based transparent conductor because divergence in resistivity should be avoided. First, we start by using widely accepted size effect models to describe the resistivity scaling of the film. Simply put, size effect models describe the increase in resistivity of the metal film as film's size (thickness or grain size) decreases. which is primarily attributed to the surface or grain boundary scattering of the conduction electrons.[26] As the details of these models can be found elsewhere,[26, 27] we will not go into details but simply use them to model our film (calculations in Section 3 of supporting information) using Matthiessen's rule as suggested by other work: [26]

$$\rho_{size} = \rho_{Surf} + \rho_{GB} - \rho_i \quad (1)$$

where ρ_{Surf} and ρ_{GB} are resistivity contribution due to surface and grain boundary scattering, respectively, and ρ_i is the bulk resistivity. Blue dotted line in **Figure 1(b)** is the approximated resistivity ($\rho_{approx.}$) of Ag (Cu) thin metal film calculated by size effect models called ρ_{size} which shows good agreement with experimental data (symbol) for thickness of d > 5 nm but fails for thickness below d < 5 nm. It can be inferred that different scattering mechanism may be limiting the electron conductivity below 5 nm. As top-down SEM images for selected film thickness show as inset of Figure 1(b), film's morphology below 5 nm can be treated as inhomogeneous medium comprised of metal film with air voids. Effective thickness d_{eff} will be used from now to define the nominal thickness of metal films. Resistivity of such inhomogeneous medium is known to scale as the fraction of air (insulator) in the medium is increased, which can be modeled using effective medium approaches.[28, 29] We extend the general effective media (GEM) theory as an empirical model to fit our data because this model entails both aspect of effective medium approximation and percolation model, which fully describes the rapid resistivity change for a wide range of metal-air composite.[30] This is appropriate for our case as we are dealing with rapid resistivity change in the vicinity of percolation threshold with different resistivity scaling behaviors. The resistivity as determined by GEM (ρ_{GEM}) model can be calculated from its conductivity σ_{GEM} (= $1/\rho_{GEM}$) as:[29]

$$(1-\phi)\cdot\frac{\sigma_m^{-t}-\sigma_{GEM}(\phi)^{-t}}{\sigma_m^{-t}+A\cdot\sigma_{GEM}(\phi)^{-t}}+\phi\cdot\frac{\sigma_0^{-t}-\sigma_{GEM}(\phi)^{-t}}{\sigma_0^{-t}+A\cdot\sigma_{GEM}(\phi)^{-t}}=0 \quad (2a)$$

$$A = \frac{1-\phi_c}{\phi_c} \quad (2b)$$

where ϕ is the metal fraction, σ_0 is the bulk conductivity of metal, t is the critical exponent of conductivity, ϕ_c is percolation threshold fraction, A is a constant, σ_m is the conductivity of the medium which can be approximated as ~ 0 (for insulator). For our case, $t = 3.06 \pm 0.2$ with percolation threshold value ϕ_c of 0.59 were empirically extracted from Ag (Cu) film's physical parameters (Figure S5a for details). In its original form **Equation 2a** does not have any dependence on the film thickness, but only the metal fraction with its bulk conductivity σ_0. To obtain explicit film thickness dependence required in this study, we extend the GEM model by choosing σ_0 to be σ_{size} (= $1/\rho_{size}$), where σ_{size} is determined by the size effect model which is a function of the film thickness. By doing so, we can dynamically capture the change in resistivity as film size shrinks to ultrathin regime. This is important because the conduction of the electron at such thin regime cannot be described in a piecewise manner, but two mechanisms are interlinked to determine the total resistivity. Resistivity value approximated by this extended GEM model $\rho_{ext.GEM} = 1/\sigma_{ext.GEM}$ is plotted as red dashed line in Figure 1(b). Surprisingly, it shows that using *GEM model with the simple substitution of* ρ_0 *by* ρ_{size} *provides an excellent fit for the experimental data throughout the entire thickness range, including the* d_{eff} *< 5 nm regime*. Also note that for the range of film thickness sufficiently large where the film is free of voids ($\phi = 1$), $\rho_{ext.\ GEM}$ naturally converges to ρ_{size}. The discrepancy arises if we assume a constant resistivity ρ_0 (=$1/\sigma_0$) throughout the entire range of $\phi(d_{eff})$ which may not be correct because the scattering at grain boundary or surfaces still plays a role at this regime (Section 5 of supporting information for details). Resistivity contribution by other mechanisms such as tunneling at discontinuous films [27, 31] have been ruled out because these models yield resistivity at least few orders of magnitude higher.

2.3. Implication of critical thickness

Despite divergence of resistivity at metal-insulator transition regime is a widely studied topic in the thin film community,[22, 29, 32] less efforts were made to study the resistivity change near critical thickness. Here we want to pay attention to the change in electrical and optical properties near critical thickness d_c to gain some engineering insight, which will be helpful in

utilizing the ultra-thin metal film as transparent conductor and for other optoelectronic applications.

First, carrier conduction mechanism undergoes a transition with respect to d_c. This is shown in **Figure 2(a)** where left axis is the modeled resistivity and the right axis is the contribution of size effect over total resistivity shown as ρ_{size}/ρ_{total} (where $\rho_{total} = \rho_{ext.GEM}$) as a function of d_{eff}. In the graph, d_c is represented as a solid vertical line. Note that, log scale plot of ρ_{size}/ρ_{total} (%) shows a rapid decrease below d_c, conversely indicating that the electron conduction is strongly influenced by inhomogeneity of the film. In fact, the measured electron scattering time τ ($= \mu \cdot m_e/q$, μ is mobility, q is charge, m_e is effective electron mass in silver where $1.03 \times m_0$ was used [33]) rapidly decays below d_c which is plotted in **Figure 2(b)** with symbol.

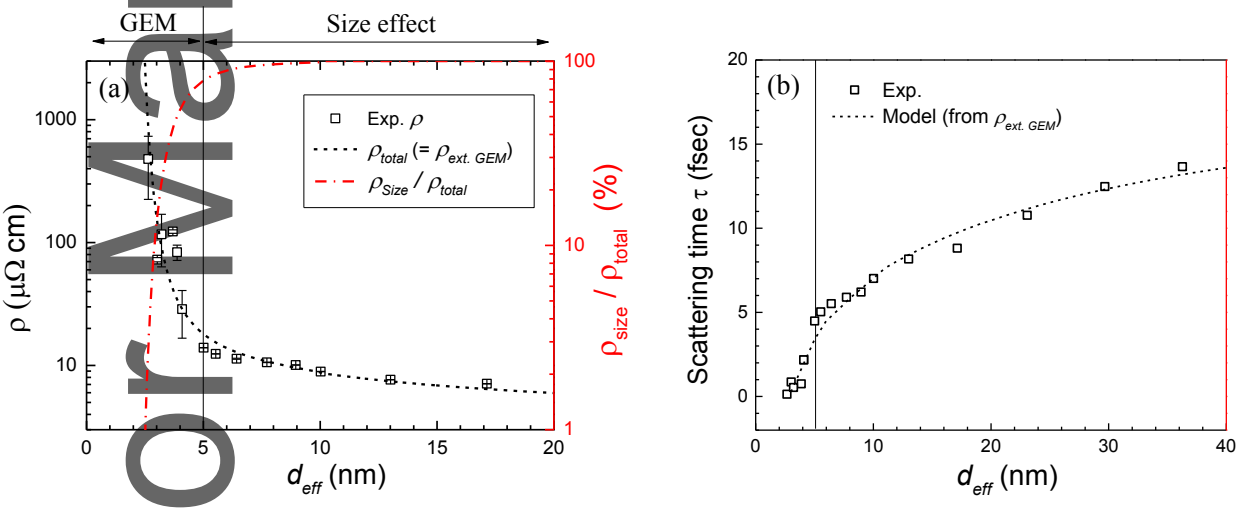

Figure 2. (a) Ag (Cu) film's total resistivity ρ_{total} ($= \rho_{ext.GEM}$, dashed black line) on the left axis and contribution of size effect model over total resistivity, ρ_{size}/ρ_{total} (dashed-dot red line) on the right axis both as a function of film thickness d_{eff}. Symbols on left axis are measured experimental resistivity values. Transport mechanism above and below critical thickness d_c (= 5nm) are each governed by size effect theory and GEM, respectively. (b) Experimental (symbol) and modeled (dashed line) carrier scattering time τ of Ag (Cu) film as a function of d_{eff}. In both figures, Ag (Cu) film's d_c is indicated as a vertical solid line.

This is attributed to the increase in metal-air interfaces due to the inhomogeneity of film, in which electron transport are impeded at these interfaces causing mean scattering time to decrease and resistivity to increase. For the film thickness above d_c, τ gradually decays as

thickness shrinks which is expected per size effect theory with the value of τ being consistent with those reported elsewhere.[34] If we assume constant carrier concentration N_c and electron mass (N_c of 5.85×10^{22}cm^{-3} [33]) within the metal phase, the overall trend of τ can be approximated by using extended GEM model $\tau^{-1} = \rho_{ext.GEM} \cdot N_c \cdot q^2/m_e$ and is plotted as black dotted line in Figure 2(b). Interestingly, Drude model (in size effect model) remains valid even for an inhomogeneous film when taking into account the reduced scattering time.

To better understand how film's morphological change affect resistivity near d_c, effective mean free path of electron l ($= \tau \cdot v_F$) was calculated using τ from $\rho_{ext.GEM}$ and Fermi velocity v_F of 14.5x10^5 m/sec [35] and plotted in **Figure 3** with symbol. If we simplify our problem by assuming that grain boundaries dominate the electron scattering in the size effect model (see Figure S3), the effective mean free path will be determined by the average grain size D because electron will scatter at each grain boundary as it travels. Also, as D is known to proportionally scale with film's thickness for a physical vapor deposited metal films,[36] we will also assume this proportionality relation ($d_{eff} \sim D$) to be valid for our case, which is an important premise for resistivity scaling due to the size effect (i.e. grain boundary scattering) model. If so, it would be the point at which l becomes smaller than D (or d_{eff}) where the size effect theory no longer becomes the dominant contributor of scattering events. As shown in Figure 3, l coincides with d_{eff}~D relation (red dotted line) for above d_c, which implies that the scattering event is governed by size effect model. This is illustrated in top-right schematic of Figure 3 which shows top-down view of film densely packed with metal-clusters with l determined by the grain size. However, l starts to deviate from $d_{eff} \sim D$ relation for below d_c. This is due to the increased metal-air (insulator) boundaries perpendicular to the direction of electric field causing diffusive reflection of electron, thus reduce l to below the size of grain boundary (top-left schematic of Figure 3). Therefore, it is easy to see that d_c is simply the thickness at which film transitions from quasi-continuous to continuous state. Resistivity scaling transitions at d_c is the result of the inhomogeneity of metal film leading to more rapid increase of the resistivity when its thickness decreases below d_c. Moreover, the resistivity below d_c tends to have large sample-to-sample variation due to the randomness of quasi-continuous film. This could raise a practical concern on the uniformity of the sample as it would mean that resistivity becomes uncontrollable as film gets thinner. Thus, one need to consider metal films with thickness above d_c for practical electronic applications.

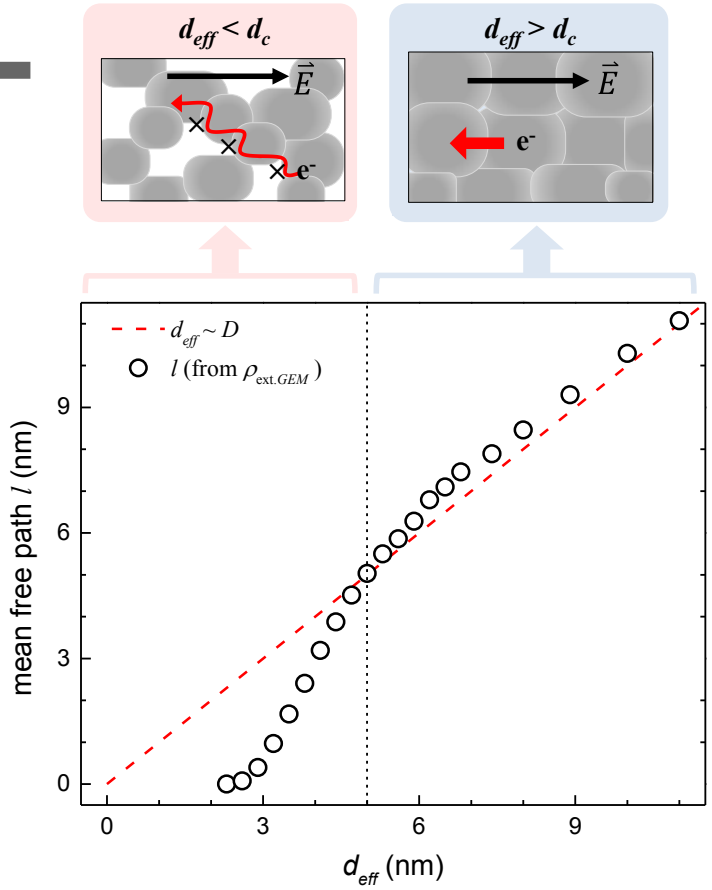

Figure 3. Film's predicted effective mean free path l (symbol) as a function of d_{eff} calculated from $\rho_{ext.GEM}$. Proportionality relation of grain size D with d_{eff} is plotted (red dashed line) as well to illustrate the size effect theory. Ag (Cu) film's critical thickness d_c (= 5nm) is indicated as a vertical dotted line. Schematics above represent top-down nanoscopic view of film's morphology in relation with the l and D for the thickness regime below (left, red) and above (right, blue) d_c. Granular shapes represent metal grains and red arrow indicates the path of traveling electron under the presence of electric field $\vec{E}$ (black arrow). Left schematic illustrates co-existence of metal clusters and air (void) depicting the inhomogeneity of the film when d_{eff} is below d_c. Each air-metal boundary (marked as cross) acts as a strong scattering site. Right schematic illustrates the homogeneous metal film free of voids when d_{eff} is above d_c.

Another important implication of critical thickness is that the film's optical property also changes its trend at d_c. **Figure 4(a)** shows the average absolute transmission (T_{AVE}) and absorption (A_{AVE}) of the Ag (Cu) film on glass substrate in the visible wavelength

range (380 – 780 nm). Note the film's optical transmission gradually increases as the film's thickness is reduced to d_c. This is anticipated because metal film can transmit electromagnetic wave when its thickness is less than the skin depth at visible frequency (~30nm for Ag [37]). As the film's thickness is further reduced to below d_c, T_{AVE} reaches a plateau followed by increase in the film's absorption. This may be due to the increased absorption (and scattering) of light by metal cluster network due to excitation of localized surface plasmon resonance. For most photonic or optoelectronic applications of metal films, it is desirable to suppress optical loss and maximize transmission, in which d_c may be used as a design criterion in determining the metal film's thickness to maximize the performance.

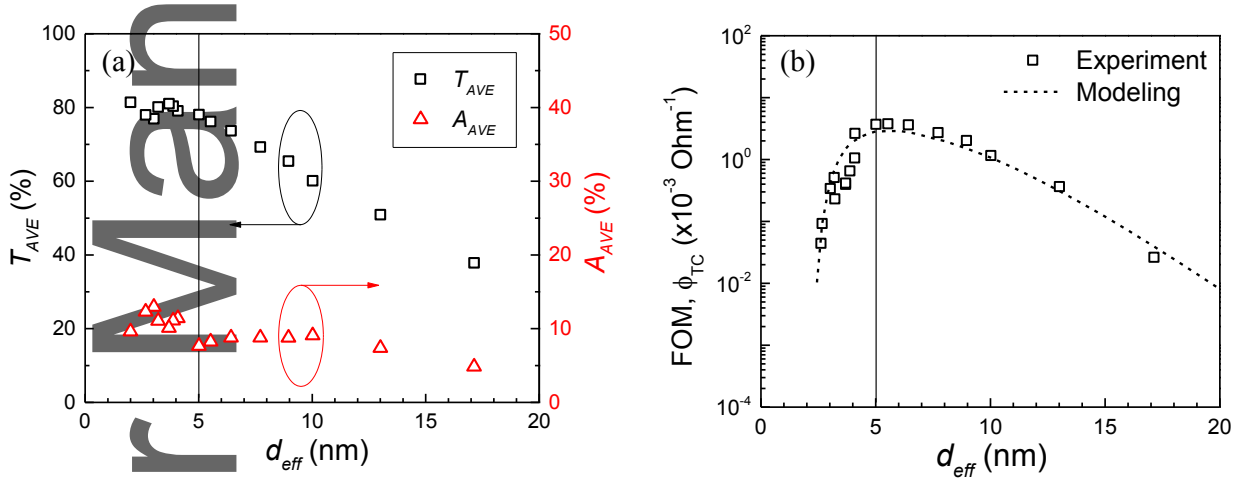

Figure 4. (a) Film's measured average transmission (T_{AVE}) and absorption (A_{AVE}) over visible wavelength (380 – 780 nm) plotted as a function of d_{eff}. (b) Haacke's figure-of-merit ϕ_{TC} (= T^{10}/R_s) of Ag (Cu) film as a function of d_{eff} where T is transmission at 550 nm wavelength and R_s is sheet resistance. Symbols and dotted line are experimental and modeled ϕ_{TC}, respectively. For modeling of ϕ_{TC}, R_s was calculated from approximation (using $\rho_{ext.GEM}$) used in Figure 1(b) and T is calculated from measured Ag (Cu) film's optical constants using transfer-matrix method. In both figures, Ag (Cu) film's critical thickness d_c (= 5nm) is indicated as a vertical solid line.

The performance of transparent conductor is typically characterized by Haacke's figure-of-merit (FoM) ϕ_{TC} $(= T^{10}/R_s)$ [38] where T is the transmittance at wavelength of 550 nm and R_s $(= \rho/d)$ is the sheet resistance. From the above discussion, one can expect an interesting aspect of d_c for the Ag (Cu) film: its FoM will reach maximum value at this

thickness. **Figure 4(b)** plots the measured (symbol) and modeled (dotted line) ϕ_{TC} of Ag (Cu) film on a substrate as a function of film thickness. To model ϕ_{TC} for Ag (Cu) film, the electrical resistivity was calculated from the resistivity approximated from red dashed line in Figure 1(a) using $\rho_{ext.GEM}$ while optical transmission T was simulated from the measured refractive index of the film by using transfer matrix method. As the results in Figure 4(b) show, the measured ϕ_{TC} of the film shows a bell-shaped curve as a function of film's thickness in which the curve is well approximated by the modeled curve. Indeed, the film's ϕ_{TC} reaches maximum value roughly at a thickness of d_c (= 5 nm). This is anticipated because below this critical thickness, the resistivity rapidly increases while the film's optical transmittance reaches plateau. For the film thickness greater than d_c, though resistivity decreases but the film becomes too thick to effectively transmit visible light, leading to a decrease in ϕ_{TC}. Therefore, it is desirable for metal film to be as thin as possible to maximize optical transmission but right before it enters quasi-continuous film at which both electrical and optical properties start to deteriorate.

Similar observation of associating percolation threshold with optimum ϕ_{TC} thickness was made elsewhere,[20] but we think the use of the term "percolation threshold" may not be accurate in this case. Percolation threshold is an important terminology to describe the change in morphology of the film growth, and it was calculated to be 2.4 nm in our case (calculation in Section 4 of supporting information). Clearly such percolation threshold is different from the thickness at which optimal FoM for a transparent conductor is obtained. Strictly speaking, percolation threshold is the point at which metal-to-insulator transition occurs which should be lower than d_c where transition from continuous to quasi-continuous state occurs. Ideally, it is important to make this d_c as low as possible to achieve maximum performance of metal film as a transparent conductor. However, making d_c too small will increase the sheet resistance of the film, which can deteriorate transparent conductor performance. For example, even when we assume ideal case of Ag (Cu) film with d_c below 2 nm, our calculation shows that ϕ_{TC} still peaks at a film thickness of around 4-5 nm which decreases below this thickness due to high electrical resistance. At this film thickness regime, electrical resistance plays a dominant role in determining the transparent conductor performance and so it is critical to engineer the film to have low electrical resistance even at extremely thickness.

3. Conclusion

In summary, ultrathin Ag (Cu) film's electrical and optical properties were studied with respect to the critical thickness d_c. For film's thickness below d_c, its electrical resistivity exponentially increases which is attributed to the rise in morphological inhomogeneity of the film. Good approximation of electrical resistivity near d_c using a slightly modified GEM model by treating the film as metal-air composite medium indicates that the film's resistivity is strongly influenced by its morphological change. First, below d_c, the conduction of electron was shown to be strongly influenced by the inhomogeneous nature of metal film which increases the scattering time. Second, the film's optical transmittance plateaus while absorption increase below d_c. Finally, as one promising application of ultrathin metal films, Ag (Cu) film's FoM as a transparent conductor reaches maximum value at d_c, which serves as an important engineering and design metric.

4. Experimental Method

In this study, Ag film was deposited on a fused silica substrate where 5Å Cu was used as a seed-layer to promote the wetting of Ag film, which will be referred as Ag (Cu) film throughout this paper. This seeded growth of Ag (Cu) film enables smooth and continuous Ag film down to extremely thin regime. The optimum thickness of Cu was chosen that guarantees Ag film with low electrical and optical loss with minimum surface roughness. Silica with size of 2 cm by 2 cm was used as a substrate for depositing Ag (Cu) film. The Ag (Cu) films were deposited using physical vapor deposition under base pressure of 10^{-7} Torr at room temperature (Kurt J. Lesker Co, LAB 18 & PVD-75). The film's resistivity was measured using 4-point-probe method (Miller Design & Equipment FPP-5000) and was cross-checked with Hall measurement (Ecopia HMS-3000) where the values were consistent within 10% of range. For Hall measurement, samples were measured with and without applying InGa Euctetic on four corners of sample which showed negligible difference. Also, ohmic contact of each sample for Hall measurement was verified by checking linearity of all four configuration of current-voltage characteristics including films near critical thickness. For the thickness range dealt in this work all showed metallic behavior while those thickness near 2 nm was not considered in the data as these films showed non-ohmic behavior exhibiting resistivity values that are few orders of magnitude higher than what is dealt here.

Minimum of three samples were prepared for a given thickness where the resistivity value of each sample was obtained from the average of five different measurement data. The film's thickness was measured via ellipsometer (Woollam M-2000) which was then cross-checked using X-ray reflectivity (XRR, Rigaku SmartLab), showing consistency in the result. Film's transmission and reflection spectra was obtained using spectroscopic ellipsometer and reflectometer (F20, Filmetrics), respectively. For transmission electron microscopy (TEM) analysis, Ag film samples were directly deposited on a Silicon Dioxide Support Films TEM grid (PELCO, 18nm, 60 x 60μm apertures (24) on 0.5 x 0.5mm Window, Ø3mm). Then, top-down images were taken under TEM bright field image mode (JEOL 2010F) with 200 kV high voltage condition. In the TEM image of Ag films, the dark contrast is diffraction contrast due to strong electron diffraction from Ag grains, indicating regions covered with Ag. Region appearing as bright spot is a sign of amorphous behavior, in which region above cutoff value was treated as a void region with no Ag. Images were obtained and processed to extract the projected area fraction ratio of metal-insulator composite films for an extremely thin film regime. For each thickness value, images were taken from at least 8 different locations of the film and the area fraction value was averaged over these images.

Supporting Information

Supporting Information is available from the Wiley Online Library or from the author.

Acknowledgements

This work is supported in part by MTRAC and Zenithnano. YBP acknowledges technical support from the Michigan Center for Materials Characterization. This work was performed in part at the University of Michigan Lurie Nanofabrication Facility.

Conflict of Interest

Authors have no conflict of interest to declare.

References

[1] S. M. Rossnagel, T. S. Kuan, Journal of Vacuum Science & Technology B: Microelectronics and Nanometer Structures Processing, Measurement, and Phenomena 2004, 22, 240; M. Guilmain, T. Labbaye, F. Dellenbach, C. Nauenheim, D. Drouin, S. Ecoffey, Nanotechnology 2013, 24, 245305; E. Ando, M. Miyazaki, Thin Solid Films 2008, 516, 4574.

[2] C. Ji, D. Liu, C. Zhang, L. Jay Guo, Nature Communications 2020, 11, 3367.

[3] C. Zhang, C. Ji, Y.-B. Park, L. J. Guo, Advanced Optical Materials 2021, 9, 2001298.

[4] A. Anders, E. Byon, D.-H. Kim, K. Fukuda, S. H. N. Lim, Solid State Communications 2006, 140, 225; V. J. Logeeswaran, N. P. Kobayashi, M. S. Islam, W. Wu, P. Chaturvedi, N. X. Fang, S. Y. Wang, R. S. Williams, Nano Letters 2009, 9, 178.

[5] Y.-G. Bi, J. Feng, J.-H. Ji, Y. Chen, Y.-S. Liu, Y.-F. Li, Y.-F. Liu, X.-L. Zhang, H.-B. Sun, Nanoscale 2016, 8, 10010.

[6] X. Yang, P. Gao, Z. Yang, J. Zhu, F. Huang, J. Ye, Scientific Reports 2017, 7, 44576.

[7] G. Zhao, W. Shen, E. Jeong, S.-G. Lee, S. M. Yu, T.-S. Bae, G.-H. Lee, S. Z. Han, J. Tang, E.-A. Choi, J. Yun, ACS Applied Materials & Interfaces 2018, 10, 27510.

[8] C. Zhang, N. Kinsey, L. Chen, C. Ji, M. Xu, M. Ferrera, X. Pan, V. M. Shalaev, A. Boltasseva, L. J. Guo, Advanced Materials 2017, 29, 1605177.

[9] H. Wang, C. Ji, C. Zhang, Y. Zhang, Z. Zhang, Z. Lu, J. Tan, L. J. Guo, ACS Applied Materials & Interfaces 2019, 11, 11782; N. Erdogan, F. Erden, A. T. Astarlioglu, M. Ozdemir, S. Ozbay, G. Aygun, L. Ozyuzer, Current Applied Physics 2020, 20, 489.

[10] F. Moresco, M. Rocca, T. Hildebrandt, M. Henzler, Physical Review Letters 1999, 83, 2238.

[11] G. Fahsold, M. Sinther, A. Priebe, S. Diez, A. Pucci, Physical Review B 2002, 65, 235408.

[12] Y.-G. Bi, Y.-F. Liu, X.-L. Zhang, D. Yin, W.-Q. Wang, J. Feng, H.-B. Sun, Advanced Optical Materials 2019, 7, 1800778.

[13] J.-W. Park, G. Kim, S.-H. Lee, E.-H. Kim, G.-H. Lee, Surface and Coatings Technology 2010, 205, 915.

[14] D. S. Hecht, L. Hu, G. Irvin, Advanced Materials 2011, 23, 1482.

[15] B. Bari, J. Lee, T. Jang, P. Won, S. H. Ko, K. Alamgir, M. Arshad, L. J. Guo, Journal of Materials Chemistry A 2016, 4, 11365.

[16] C. Jeong, Y.-B. Park, L. J. Guo, Science Advances 2021, 7, eabg0355.

[17] D. Zhang, H. Yabe, E. Akita, P. Wang, R.-i. Murakami, X. Song, Journal of Applied Physics 2011, 109, 104318.

[18] A. I. Maaroof, B. L. Evans, Journal of Applied Physics 1994, 76, 1047.

[19] N. Formica, D. S. Ghosh, A. Carrilero, T. L. Chen, R. E. Simpson, V. Pruneri, ACS Applied Materials & Interfaces 2013, 5, 3048; S. Jeong, S. Jung, H. Kang, D. Lee, S.-B. Choi, S. Kim, B. Park, K. Yu, J. Lee, K. Lee, Advanced Functional Materials 2017, 27, 1606842.

[20] D. S. Ghosh, T. L. Chen, V. Pruneri, Applied Physics Letters 2010, 96, 091106.

[21] D. S. Ghosh, T. L. Chen, N. Formica, J. Hwang, I. Bruder, V. Pruneri, Solar Energy Materials and Solar Cells 2012, 107, 338.

[22] M. Hövel, B. Gompf, M. Dressel, Physical Review B 2010, 81, 035402.

[23] C. Zhang, Q. Huang, Q. Cui, C. Ji, Z. Zhang, X. Chen, T. George, S. Zhao, L. J. Guo, ACS Applied Materials & Interfaces 2019, 11, 27216.

[24] E. V. Barnat, D. Nagakura, P. I. Wang, T. M. Lu, Journal of Applied Physics 2002, 91, 1667.

[25] N. Chuang, J. Lin, T. Chang, T. Tsai, K. Chang, C. Wu, IEEE Journal of the Electron Devices Society 2016, 4, 441.

[26] T. Sun, B. Yao, A. P. Warren, K. Barmak, M. F. Toney, R. E. Peale, K. R. Coffey, Physical Review B 2010, 81, 155454.

[27] M. A. Angadi, Journal of Materials Science 1985, 20, 761.

[28] M. H. Cohen, J. Jortner, I. Webman, Physical Review B 1978, 17, 4555; P. M. Kogut, J. P. Straley, J. C. Garland, D. B. Tanner, AIP Conference Proceedings 1978, 40, 382; R. Landauer, Journal of Applied Physics 1952, 23, 779.

[29] D. S. McLachlan, M. Blaszkiewicz, R. E. Newnham, Journal of the American Ceramic Society 1990, 73, 2187.

[30] M. Taya, *Electronic Composites: Modeling, Characterization, Processing, and MEMS Applications*, Cambridge University Press, 2005.

[31] G. Dittmer, Thin Solid Films 1972, 9, 317; P. Sheng, B. Abeles, Physical Review Letters 1972, 28, 34.

[32] A. L. Efros, B. I. Shklovskii, physica status solidi (b) 1976, 76, 475.

[33] C. Kittel, *Introduction to Solid State Physics*, Wiley, 2004.

[34] G. Ding, C. Clavero, D. Schweigert, M. Le, AIP Advances 2015, 5, 117234.

[35] D. Gall, Journal of Applied Physics 2016, 119, 085101.

[36] A. F. Mayadas, R. Feder, R. Rosenberg, Journal of Vacuum Science and Technology 1969, 6, 690; K. N. Tu, A. M. Gusak, I. Sobchenko, Physical Review B 2003, 67, 245408; M. Philipp, in *Fakultät Mathematik und Naturwissenschaften*, Vol. PhD, Technische Universität Dresden, 2011.
[37] Y. Li, *Plasmonic Optics: Theory and Applications*, SPIE Press, 2017.
[38] G. Haacke, Journal of Applied Physics 1976, 47, 4086.

We observe a rapid increase in electrical resistivity of ultrathin Ag film below its critical thickness where its resistivity is strongly influenced by film's morphology which can be modeled by extended general effective media theory. The critical thickness of metal film can serve as important engineering metric for its use as a transparent conductor application.

Yong-Bum Park, Changyeong Jeong, and L. Jay Guo*

Resistivity scaling transition in ultrathin metal film at critical thickness and its implication for the transparent conductor applications